Polyhedron 253 (2024) 116927

Contents lists available at ScienceDirect

Polyhedron

journal homepage: www.elsevier.com/locate/poly

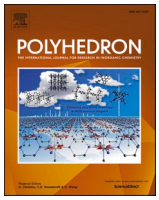

Investigating aging processes and characterization of nanodispersed Cu-Al layered double hydroxides produced by non-equilibrium electrochemical oxidation

Natalia V. Usoltseva [a], Johannes H. Potgieter [b,c,*], Vladimir V. An [a], Baodan Liu [d], Sergey A. Stepanov [e], Damir T. Valiev [e]

[a] Kizhner Research Center, School of Advanced Manufacturing Technologies, Tomsk Polytechnic University, 30 Lenin Ave., Tomsk 634050, Russia
[b] Department of Natural Sciences, Manchester Metropolitan University, Manchester M15 6GD, UK
[c] School of Chemical and Metallurgical Engineering, University of the Witwatersrand, Private Bag X3, Wits, 2050, South Africa
[d] Foshan Graduate School of Innovation, Northeastern University, No.2, Zhihui Road, Foshan 528300, China
[e] Division of Materials Science, School of Advanced Manufacturing Technologies, Tomsk Polytechnic University, 30 Lenin Ave., Tomsk 634050, Russia

ARTICLE INFO

Keywords:
Electrochemical metal oxidation
Phase composition
Materials characterization
Layered double hydroxide
Aging
Cu-Al/LDH

ABSTRACT

The present paper describes an investigation of aging processes and the characterization of nanodispersed materials prepared by non-equilibrium electrochemical oxidation of metals. X-ray diffraction (XRD), differential scanning calorimetry (DSC), transmission electron microscopy (TEM) analyses, and the reflectance spectra investigation were used to characterize the electrolysis products aged naturally over time. The ageing of electrolysis products in the solution leads to the conversion of Cu_2O-AlOOH into Cu-Al layered double hydroxides (Cu-Al-CO_3-LDH) and $Cu_2(OH)_2CO_3$ due to the Jahn-Teller effect. Long-term aging results in: (i) stability of phase composition but a slight increase of the interplanar spacing due to the sorption ability of the nanostructures in air; (ii) temperature decrease of Cu-Al-CO_3-LDH decomposition from 135 to 121 °C due to the stability deterioration with further content increase of carbonate ions (DSC analysis) and decrease of hydroxide ions (FT-IR analysis); (iii) 2.5 times increase of the coherent scattering region (CSR) of all copper-containing compounds compared with short-term aging (40–50 nm vs. 15–20 nm); and (iv) no size change of the flower-like Cu-Al-CO_3-LDH and dramatical size decrease of nanodispersed particles of CuO and $Cu_2(OH)_2CO_3$ because of deagglomeration. Conversion CuO/Al_2O_3 to Cu-Al-CO_3-LDH makes a positive impact on photocatalytic activity of nanodispersed materials while it results in the increase the reflection coefficient.

1. Introduction

Layered double hydroxides (LDH) is a class of synthetic anionic clays in which the structure is represented by layers similar to brucite ($Mg(OH)_2$), with some divalent cations replaced by trivalent ions [1]. These materials have attracted attention as various catalysts [2,3], chemical adsorbents [4,5], anion exchangers [6], bioactive nanostructures [7,8], electroactive, photoactive elements [9,10], and flame retardant nanocomposites [11,12]. Copper aluminum LDH can be used as electrocatalysts for the carbon dioxide reduction [13]. It has been reported that copper–aluminum layered double hydroxides are promising nanofillers in thin film nanocomposite nanofiltration membranes for water purification [14]. Cu-Al layered double hydroxides synthesis conditions are able to have an impact on selective hydrogenation of 5-acetoxymethylfurfural over Cu-based catalysts [15]. The authors [16] have successfully shown the efficient degradation of ammonia nitrogen in water with a LDH, which yielded a high removal efficiency and can be applied for the catalytic removal of water pollutants. They have also reported that the hierarchical LDH materials exhibit unusual adsorption ability through strong electrostatic attractions.

The majority of catalytic and photocatalytic materials is subject to changes of their properties over time, and their catalytic performance depend on these temporal modifications. Distinctive feature of nanomaterials is the instability of their phase composition and structure over time. It can result in the interaction of nanomaterials with some species of surrounding environment [17,18]. Changes over time, or aging, can

* Corresponding author.
E-mail address: h.potgeiter@mmu.ac.uk (J.H. Potgieter).

https://doi.org/10.1016/j.poly.2024.116927
Received 11 December 2023; Accepted 2 March 2024
Available online 9 March 2024
0277-5387/© 2024 Elsevier Ltd. All rights reserved.

affect the physical and chemical properties of LDH synthesis products, e. g. it can increase the crystallinity, as well as the cationic content, of the formed LDH [19]. Besides, there are methods that involve aging in their synthesis, like separate nucleation and aging steps (SNAS) for MgAl-LDH fabrication. During the SNAS process, rapid mixing and nucleation in a colloid mill is followed by a separate aging process [20]. Aging is typically a rather slow process. It may cause a change of phase composition and microstructure, as well as a surface change of nanoparticles. Two types of aging methods should be taken into account: short-term and long-term aging. Quite often, researchers mean short-term or long-term aging stretches from 12 to 24 h, respectively [21]. Meanwhile, new technologies of LDH nanostructured materials for photocatalytic applications also require a focus on the investigation of very long aging processes, sometimes several years. It is related to the necessity to monitor long life span performance of the LDH photocatalytic materials. Modifications in chemical composition, morphology and structure of LDH materials within long-term aging processes are of great interest in terms of their technological applications and requirements.

There are a number of methods to produce the nanodispersed oxides and multicomponent oxide materials from metals (for example, the electrochemical oxidation of metal plates [22] and the electrical explosion of metal wires [23]).

This work describes an aging investigation of the nanomaterials produced by the joint electrochemical oxidation of copper and aluminum. The results related to short-term (60 days) and long-term (5 years) changes in structural, thermochemical and photoactive properties detected using different characterization methods (X–ray diffraction, transmission electron microscopy, thermal analysis, and reflectance spectroscopy). The research work included the determination of the phase composition, morphological features, interplanar spacings, thermal effects during heating, and reflection coefficients of the aged LDH samples. This contributes new knowledge about the behavior, properties and characteristics of aged LDH materials, which can expand their potential applications in various fields, such as for example the development of high performance photoanodes or photocathodes in photoelectrochemical cells for photocatalytic water splitting and enhancing the hydrogen evolution reaction. Furthermore, these materials can find application in metal oxide nanofluids, and a thorough knowledge of their structure and properties is essential for this application.

2. Experimental

2.1. Materials and methods

Sodium chloride was purchased and used as received without further purification. Sheets of copper and aluminum were used to prepare soluble electrodes. Copper sheet of the M1 grade contains at least 99,5 % copper, aluminum sheet of the A0 grade contains at least 99 % aluminum.

X-ray diffraction (XRD) measurements were performed using an XRD-7000 diffractometer (Shimadzu), CuK_α radiation, $\lambda = 1.5418$ Å, at 30 mA and 40 kV. The data were collected from 10 to 70° 2θ at a counting rate of 2θ/min. The PDF2 database was used to identify the phase compositions. Full-profile analysis of X-ray diffraction patterns was performed with the program "Powder Cell 2.4" to determine the content of copper compounds in the samples and the crystallite size (in the coherent scattering region).

Thermogravimetric analysis (TGA) and differential scanning calorimetry (DSC) were carried out on a thermal analyzer SDT Q600 in air at a heating rate of 10 °C min^{-1} in the temperature range from ambient to 700 °C.

The FT-IR spectra were recorded on a Nicolet 5700 spectrometer equipped with a diffuse reflectance cell in the range of 4000——400 cm^{-1} at a resolution of 4 cm^{-1}.

Transmission electron microscopy (TEM) analysis was carried out on JEOL JEM-2100F to evaluate surface morphology of the samples.

The reflectance spectra of investigated samples were measured using an AVASPHERE-50-LS-HAL integrating sphere and Avantes AvaSpec-3648 fiber spectrometer in the 200–1000 nm spectral range. A Xenon 150 W light source with an operating range of 200–2500 nm was used as a source of probing radiation. A MS-20 glass reference was applied to reduce the effect of reflection from the sample surface.

2.2. Synthesis of copper-containing powders

Both copper and aluminum plates were jointly electrochemically oxidized. The density of alternating current of industrial frequency (50 Hz) was 1 A/cm^2. Electrochemical oxidation was carried out in a 3 wt% sodium chloride solution at 90 °C. These concentration and temperature are the most appropriate in terms of metal oxidation rate and energy consumption.

3. Results and discussion

3.1. Preparation of nanodispersed powders

Electrochemical co-oxidation of copper and aluminum produces the copper (I) oxide and aluminum oxyhydroxide (boehmite) [24].

Nanodispersed products of metal co-oxidation were treated in two ways.

Vacuum way: Vacuum drying of nanodispersed products of metal co-oxidation at a residual pressure of 3–4 kPa by the use of vacuum pump that was connected to a flask containing the suspension of nanodispersed products. Vacuum drying was carried out until a dry crumbly powder was done. It prevents a phase transformation of copper (I) oxide to some copper carbonates. In air the dry nanodispersed copper (I) oxide is stable against interaction with carbonate ions, but does not have resistance to oxidation; thus, copper (I) oxide is oxidized to copper (II) oxide by aging it in air.

The result of the Cu_2O oxidation depends on the Pilling–Bedworth ratio and the pore structure of the CuO. The Pilling–Bedworth ratio (P–B ratio) is the ratio of the volumes of the oxidized and the formed compounds, Cu_2O and CuO respectively [25]:

$$\alpha_{CuO/Cu_2O} = \frac{V_{CuO}}{V_{Cu_2O}} = \frac{M_{CuO}/\rho_{CuO}}{n \cdot M_{Cu_2O}/\rho_{Cu_2O}} = \frac{M_{CuO} \cdot \rho_{Cu_2O}}{n \cdot M_{Cu_2O} \cdot \rho_{CuO}}$$

where M_{CuO}, M_{Cu_2O} is the molar mass of CuO and Cu_2O, respectively, in g/mol, ρ_{CuO}, ρ_{Cu_2O} is the density of the CuO and the Cu_2O, respectively, in g/cm^3, n is the number of atoms of the formed copper compound (Cu_2O) per 1 molecule of the oxidized copper compound (CuO).

The Pilling–Bedworth ratio was calculated taking into account the true densities of copper oxides [26]. It is slightly greater than one ($\alpha = 1.05$) for oxidation of Cu_2O to CuO. The Pilling–Bedworth ratio is in the range from 1 to 2, and therefore the CuO coating should provide protection against further oxidation of the surface. However, there is a difference between the true density and envelope density, because the envelope density includes pores in the material. In addition, CuO layer on a curved nanoparticle surface tend to be destructed due to the mechanical stresses that increase as the surface curvature become larger. These prevent any CuO protection effect and create conditions favorable for further Cu_2O oxidation. This is why Cu_2O is completely oxidized to CuO.

Air way: Air drying of nanodispersed products of metal co-oxidation results in the formation of copper carbonate hydroxide and Cu-Al-CO_3-layered double hydroxide [24].

Copper-aluminum layered double hydroxide (LDH) has a hydrotalcite-like structure of the general formula $[M^{2+}_{1-x}M^{3+}_{x}(OH)_2]^{x+}\hat{A}\cdot[A^{n-}_{x/n}\hat{A}\cdot yH_2O]^{x-}$ [1]. The structure of such compounds is derived from the structure of brucite: part of the M^{2+} ions in

the octahedral positions of the hydroxide layers is isomorphically replaced by M^{3+} ions. Because of this, the layers have a positive charge, which is neutralized by anions located between the layers. There are two conditions for such structures to be stable [1]: (i) radii of M^{2+} and M^{3+} ions differ by less than 30 %; (ii) radii of M^{2+} and M^{3+} ions are less than 0.07 nm.

The radii of Cu^{2+} and Al^{3+} ions are 0.073 and 0.054 nm [27], respectively, and differ by 35 %. Despite the fact that both conditions are not met, layered double hydroxides of copper and aluminum can be synthesized [28]. The stability of such structures is a result of the octahedral distortion around the copper ion and degeneracy removal of the electronic state by lowering the symmetry (the Jahn-Teller effect). The layers of the LDH structure are deformed, and this stabilizes the structure of the layered double hydroxide containing copper ions [1]. However, the deformation of the layers reduces the stability of the structure. Thus, only a low content of copper ions is required to get a stable LDH. As a result, at a high copper ions content, the copper carbonate hydroxide (malachite, $Cu_2(OH)_2CO_3$) is formed along with layered double hydroxides [28]. The higher stability of $Cu_2(OH)_2CO_3$ is due to the fact that the layered structure of $Cu_2(OH)_2CO_3$ is more flexible because the octahedrons in the layers are connected by their edges, not by faces as in LDH, and there is no need for the octahedron to be disordered in the layered structure of $Cu_2(OH)_2CO_3$. The copper carbonate hydroxide is formed at a low pH, and the layered double hydroxide of copper and aluminum is formed at an elevated pH [29].

The samples after vacuum and air drying were stored in close vessels at both short-term and long-term aging.

3.2. XRD analysis

Figs. 1 and 2 show that both ways of treatments did not change the phase composition when aging occurs.

XRD patterns of nanopowders after vacuum drying and aging for a different period of time are shown in Fig. 1.

A comparison of the XRD patterns reveals that there is no phase composition change after long-term aging. After aging for 5 years (long-term aging), the peaks of copper (II) oxide and boehmite (the product of the co-oxidation of copper and aluminum) are shifted towards smaller values of 2θ. The increase of interplanar spacing (Tables 1 and 2) results from the sorption ability of the nanostructures in air. It does not form new phases, but merely experience a structural change.

The XRD patterns of the nanopowders after air drying are shown in Fig. 2. Except for the (200) plane, the interplanar spacing of the nanodispersed Cu-Al-CO_3-LDH after short-term aging is larger than the interplanar spacing of Cu-Al-CO_3-LDH according to the literature PDF No. 00–046-0099 (Table 3). All interplanar spacing of $Cu_2(OH)_2CO_3$ is also more than the literature ones according to PDF No. 00–041-1390 (Table 4). Long-term aging leads to a shift and widening of the peaks of copper-containing compounds ($Cu_2(OH)_2CO_3$ and Cu-Al-CO_3-LDH). However, the boehmite peaks are not changed. Some peaks of $Cu_2(OH)_2CO_3$ overlapped the peaks of Cu-Al-CO_3-LDH.

The copper-containing LDHs are stable for certain ranges of the functional groups' contents. It is known, if the content of the functional groups (CO_3^{2-}, OH^-, H_2O) does not correspond to the stoichiometric composition, the interplanar spacing changes. The decrease of the interplanar spacing is a result of the lack of functional groups, whereas the increase of interplanar spacing is due to the excess of functional groups as a result of long-term aging.

Thus, the increase of interplanar spacing of the produced materials confirms that the carbonization is ongoing at long-term aging.

The change of the XRD peaks (width, intensity) confirms the transformation of the particle grains.

In contrast to the XRD patterns, the FT-IR spectra (Fig. 3) differ dramatically after long-term aging due to dehydration and interaction with the ambient medium. The main difference is a 3 times increase in the transmittance at 3300——3100 cm^{-1} because of the lack of hydroxyls connected with two and three aluminum cations (stretching vibration of ν_s Al–OH and ν_{as} Al–OH). The decrease of hydroxyl bands gives one an opportunity to detect bands of stretching OH vibrations of malachite at 3320 and 3400 cm^{-1} [30]. The broad band in the range of 2300–1800 cm^{-1} assigned to OH vibrations between layers of boehmite [31,32] has disappeared.

The absorption bands at 3735 cm^{-1} and around 1650 cm^{-1} are assigned to asymmetric stretching (ν_{as} H — O — H) and bending (δ H — O — H) vibrations of water molecules. Those bands do not disappear after long-term aging.

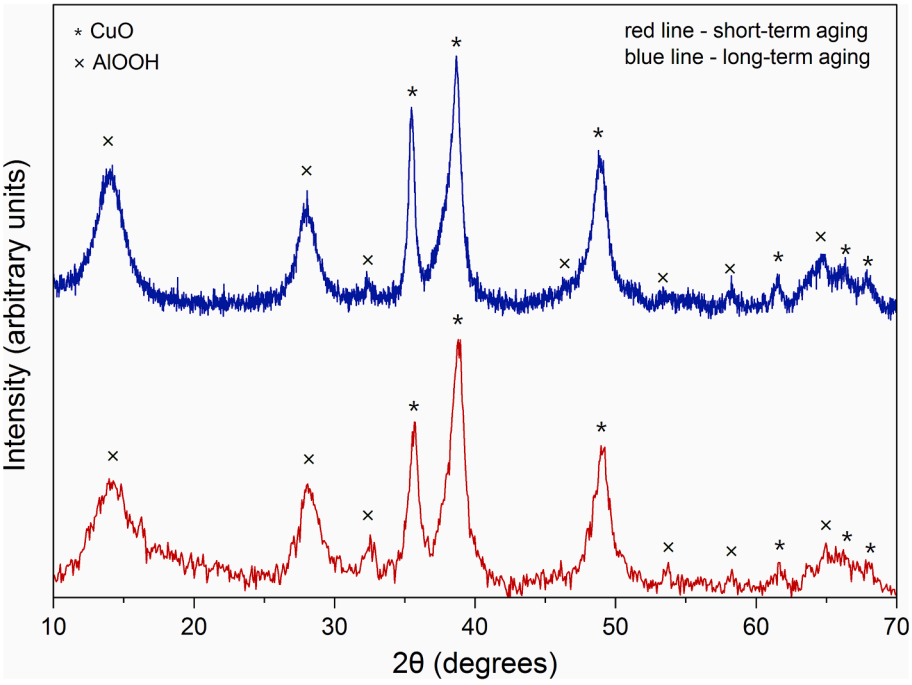

Fig. 1. XRD patterns of the nanodispersed materials produced by electrochemical oxidation of copper and aluminum (vacuum drying).

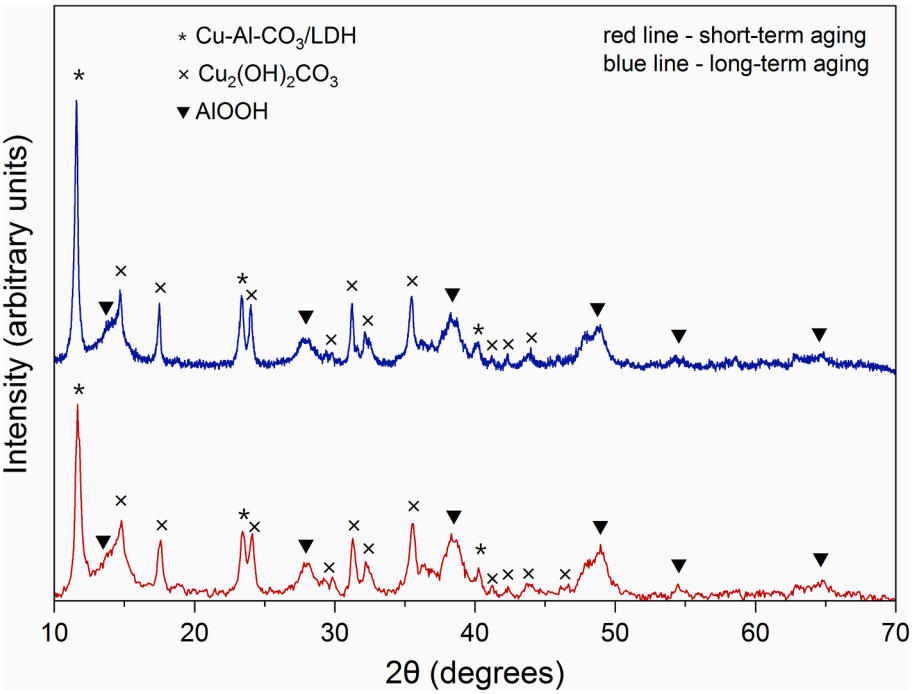

Fig. 2. XRD patterns of the nanodispersed materials produced by electrochemical oxidation of copper and aluminum (air drying).

Table 1
Interplanar spacing of nanodispersed copper (II) oxide produced by the electrochemical oxidation of copper together with aluminum (vacuum drying).

Sample	Interplanar spacing of copper (II) oxide, nm			
	(111)	(−111)	(−202)	(–222)
PDF card No. 00–005-0661	0.2524	0.2311	0.1867	0.1375
Short-term aging	0.2512	0.2313	0.1860	0.1380
Long-term aging	0.2530	0.2321	0.1867	0.1381

Table 2
Interplanar spacing of nanodispersed boehmite produced by the electrochemical oxidation of aluminum together with copper (vacuum drying).

Sample	Interplanar spacing of boehmite, nm				
	(020)	(120)	(031)	(051)	(002)
PDF card No. 00–021-1307	0.6110	0.3164	0.2346	0.1860	0.1434
Short-term aging	0.6281	0.3155	0.2359	0.1859	0.1434
Long-term aging	0.6317	0.3177	0.2360	0.1860	0.1442

Table 3
Interplanar spacing of nanodispersed Cu-Al-CO_3-layered double hydroxide produced by electrochemical oxidation of copper and aluminum (air drying).

Sample	Interplanar spacing of Cu-Al-CO_3-layered double hydroxides, nm				
	(200)	(400)	(−302)	(21–1)	(311)
PDF card No. 00–046-0099	0.7538	0.3764	0.2727	0.2515	0.2230
Short-term aging	0.7499	0.3799	0.2860	0.2522	0.2237
Long-term aging	0.7642	0.3811	0.2863	0.2529	0.2245

The band in the range of 2385–2350 cm^{-1} due to adsorbed carbon dioxide becomes much more intense. It confirms the sorption ability of nanostructured materials being investigated. At the same time, there is no change in asymmetric stretching vibration of interlaminar carbonate ν_{as} (CO_3^{2-}) at 1350 cm^{-1}.

Thus, the analysis of FT-IR spectra clearly confirms that the change of the interlayer Cu-Al-CO_3-LDH distance is caused by CO_2 uptake, not by hydration.

The coherent scattering region (CSR) of all phases of copper- and aluminum compounds was calculated using the Debye–Scherrer equation [33]:

$$D = \frac{k\lambda}{\beta\cos\Theta}$$

where k is the Scherrer constant (the typical value is 0.9), λ is the wavelength of the X-ray beam (1.5418 Å), β is the full width at half maximum intensity (FWHM), and θ is the Bragg angle.

FWHM of copper-containing compounds after short-term and long-term aging are listed in Table 5.

The CSR of boehmite and copper (I) oxide are 3–4 nm and 15–20 nm, respectively [24]. There is no CSR change of boehmite at short-term and long-term aging.

As for vacuum-dried samples, the decrease of FWHMs at the aging do not cause the dramatic change of CSR.

Concerning air-dried samples, narrowing of the diffraction peaks (Table 5) of $Cu_2(OH)_2CO_3$ and Cu-Al-CO_3-LDH is the result of long-term aging. Thus, the CSR of these compounds increased from 15 to 20 nm to 40–50 nm. In contrast to copper oxide, copper compounds are stabilized if they include carbonate ions ($Cu_2(OH)_2CO_3$ and Cu-Al-CO_3-LDH).

Table 4
Interplanar spacing of nanodispersed copper carbonate hydroxide produced by electrochemical oxidation of copper together with aluminum (air drying).

Sample	Interplanar spacing of copper carbonate hydroxide, nm					
	(020)	(120)	(220)	(040)	(20–1)	(21–1)
PDF card No. 00–041-1390	0.5970	0.5040	0.3690	0.2985	0.2861	0.2781
Short-term aging	0.5989	0.5046	0.3691	0.2996	0.2996	0.2781
Long-term aging	0.6034	0.5068	0.3705	0.3000	0.3000	0.2783

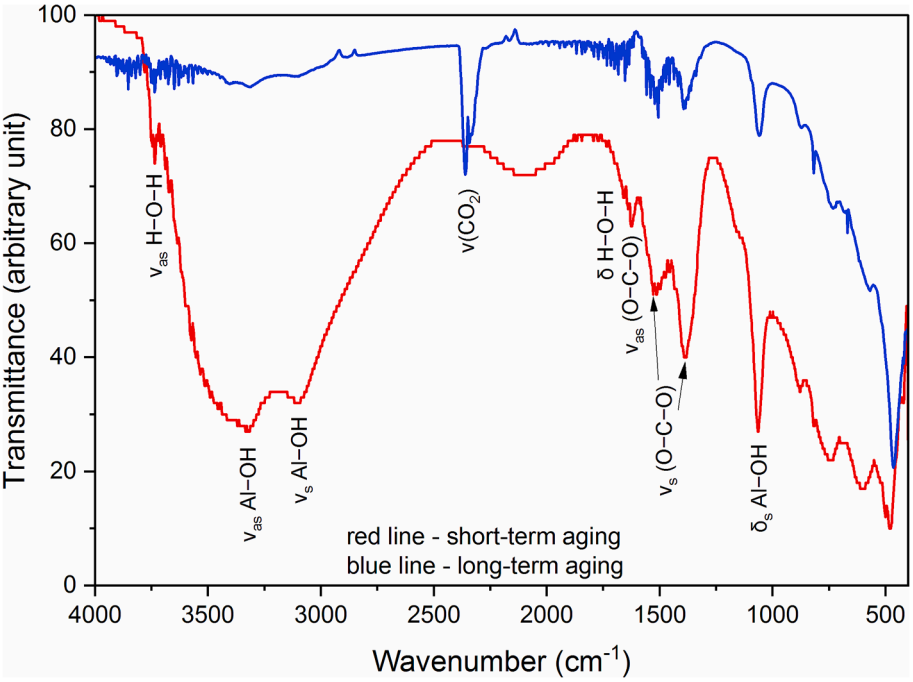

Fig. 3. FT-IR spectra of the nanodispersed materials produced by electrochemical oxidation of copper and aluminum (air drying).

Table 5
Full width half maximum (FWHM) of nanodispersed copper and aluminum compounds produced by the electrochemical oxidation of copper and aluminum (vacuum drying).

Vacuum drying (Fig. 1)					
Ageing duration	FWHM of copper (II) oxide, degree				
	(111)	(−111)	(−202)	(–222)	
Short-term aging	0.56	1.10	1.26	0.98	
Long-term aging	0.52	0.97	1.01	0.95	
Ageing duration	FWHM of boehmite, degree				
	(020)	(120)	(031)	(051)	(002)
Short-term aging	3.40	2.23	1.18	2.16	1.32
Long-term aging	2.35	1.75	1.10	1.36	1.07
Air drying (Fig. 2)					
Ageing duration	FWHM of Cu-Al-CO_3-layered double hydroxides, degree				
	(200)	(400)	(−302)	(21–1)	(311)
Short-term aging	0.50	0.79	0.35	0.33	0.36
Long-term aging	0.24	0.36	0.24	0.28	0.26

Ageing duration	FWHM of copper carbonate hydroxide, degree					
	(020)	(120)	(220)	(040)	(20–1)	(21–1)
Short-term aging	0.56	0.41	0.28	0.49	0.77	0.49
Long-term aging	0.24	0.21	0.19	0.45	0.70	0.42

3.3. Thermal analysis

Figs. 4 and 5 shows the results of the thermal analysis of the sample after vacuum and air drying, respectively. Three the same peaks can be recognized on DSC and DTG curves (I_{wt}, II_{wt}, III_{wt} and I_t, II_t, III_t). The other peaks result from the difference in sample compositions.

The overall weight loss of the sample after vacuum drying and long-term aging is 23.8 wt%. It is more than after short-term aging (19.0 wt %).

DSC and DTG curves do not strictly correlate with each other. According to the DTG curves, the aging is not followed by the temperature change of the dehydration weight loss (Fig. 4, I_{wt}), while the temperature of the endothermic peak increased from 74.7 to 93.6 °C (Fig. 4, I_t). It correlates with the absorption bands of water molecules on the FT-IR spectra (Fig. 3). The increase of the heat flow (W/g) is the result of high sorption ability of the nanostructured material when aging [34] (therefore, high heat consumption for desorption), whereas the temperature increase results from the ordering of the defect structure and decrease of high internal energy storage at the aging.

Endothermic peaks II_t and III_t (and weight loss II_{wt} and III_{wt}) are attributed to the dehydroxylation of boehmite during the conversion of boehmite to alumina (reaction (1).

$$2AlOOH = Al_2O_3 + H_2O \quad (1)$$

The peaks IV_{wt} and IV_t in the temperature range of 210–345 °C are the result of peak overlap of different processes: (i) the crystallization of nanostructured CuO (exothermic process, no weight change); (ii) boehmite decomposition (endothermic process, weight loss); (iii) the release of any species that adsorbed at long-term aging (endothermic process, weight loss).

The sharp rise of the heat release (Fig. 4, IV_t) and high weight loss (Fig. 4, IV_{wt}) after long-term aging are due to the change of the ratio of processes (i) – (iii).

The heat release is because of the endoeffect decrease of boehmite decomposition (process (ii)) whereas high weight loss corresponds to increased release of adsorbed species [35].

The weight loss in the temperature range of 210–345 °C after short-term aging is 2.2 times less than after long-term aging. Due to this, the overall weight loss depends on the aging period duration.

The overall weight loss of the nanostructures after air drying depends slightly on the duration of their aging. It is 26.8 wt% after short-term aging and 26.2 wt% after long-term aging (Fig. 5). Integral and differential curves of the weight loss reveal that aging causes a temperature change of the endothermic peaks. Comparison of the DSC and DTG curves shows that a broad peak I_t at the temperature up to 190 °C is the result of the overlap of two peaks: (i) dehydration (removal physically adsorbed water and (ii) decomposition of Cu-Al-CO_3-layered double hydroxide.

Moreover, after long-term aging there is a temperature decrease corresponding to the weight loss, from 64.5 to 47.5 °C (Fig. 5, I_{wt}) and from 135 to 121 °C (Fig. 5, V_{wt}), respectively.

Endothermic peaks II_t and III_t (and weight loss II_{wt} and III_{wt}) corresponds to the transformation of boehmite into alumina.

The Cu-Al-CO_3-layered double hydroxide is the most sensitive phase to the environment. It is because of the interaction with air (sorption of

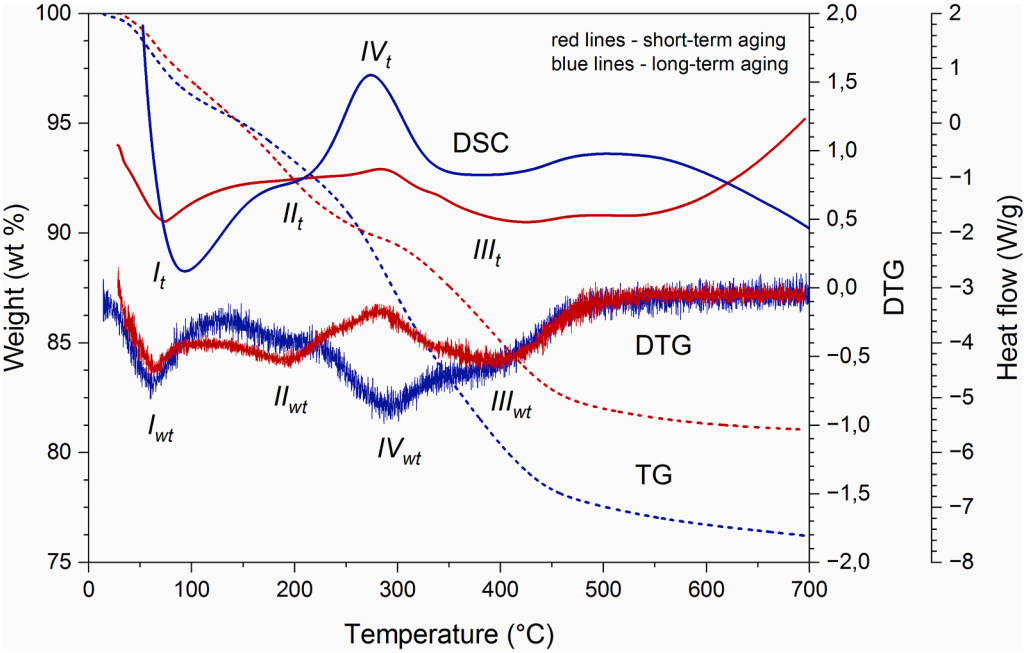

Fig. 4. DSC/DTG/TG curves of the nanostructures produced by non-equilibrium electrochemical oxidation of copper and aluminum (vacuum drying).

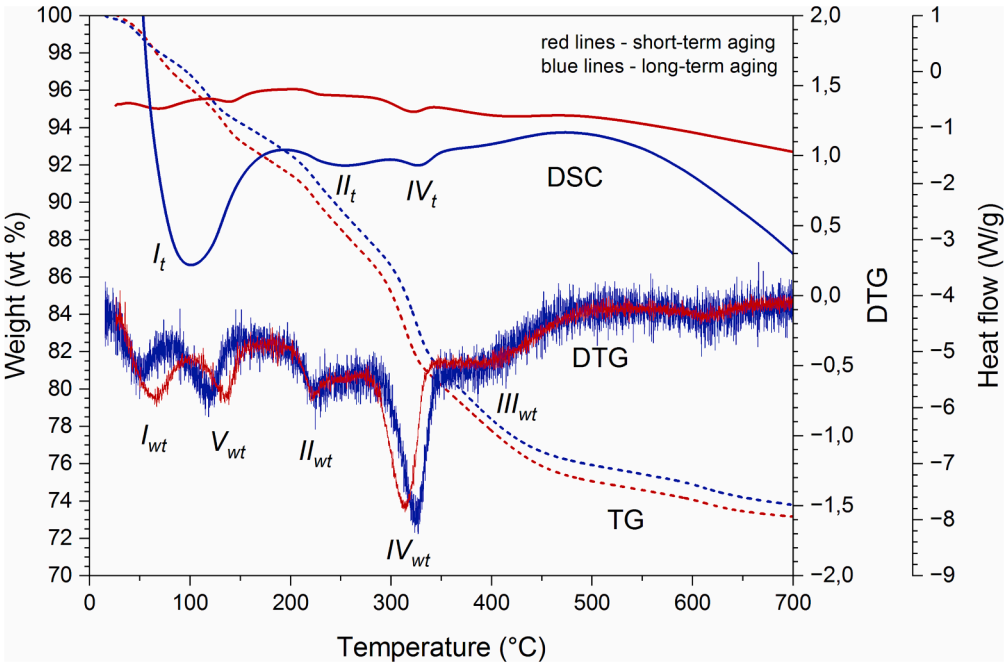

Fig. 5. DSC/DTG/TG curves of the nanostructures produced by non-equilibrium electrochemical oxidation of copper and aluminum (air drying).

air-contained compounds or desorption of some compounds in the air) that results in a change of the layered structure. The structure disordering makes decomposition easier. Therefore, the temperatures of both the water desorption and Cu-Al-CO_3-LDH decomposition decreased.

The Cu-Al-CO_3-LDH decomposition has been confirmed by comparison of the XRD pattern of the sample after short-term aging and heat treatment at both 110 and 150 °C. The XRD pattern after 150 °C does not include diffraction peaks of Cu-Al-CO_3-LDH [32]. The only weight loss in the temperature range 110–150 °C can be thoroughly assigned to the Cu-Al-CO_3-LDH decomposition. After long-term aging we also can see only one endoeffect (together with weight lost, peak V_{wt}) at the temperature range 110–150 °C. On this basis, it was reasonably assigned to the Cu-Al-CO_3-LDH decomposition.

The temperature of the first stage of $Cu_2(OH)_2CO_3$ decomposition (dehydration, reaction (2) does not changed with aging (Fig. 5, II_t), whereas the second stage of copper carbonate hydroxide decomposition (dissociation, reaction (3) after long-term aging is 323.6 °C (Fig. 5, IV_t) and higher than ones before short-term aging (312.4 °C).

$$Cu_2(OH)_2CO_3 = CuO{\cdot}CuCO_3 + H_2O \quad (2)$$

$$CuO{\cdot}CuCO_3 = CuO + CO_2 \quad (3)$$

The $Cu_2(OH)_2CO_3$ is more stable than the Cu-Al-CO_3-LDH. Thus, it is

less affected by the environment. The reasons for the temperature increase of the $Cu_2(OH)_2CO_3$ decomposition after long-term aging is a reduction in reactivity as a result of relaxation of internal stresses.

3.4. TEM analysis

The microstructure of the materials produced by non-equilibrium electrochemical oxidation of copper and aluminum is covered elsewhere [36]. The particle size is much larger than the coherent scattering region of all the phases. The particle morphology depends on the phase composition. Long-term aging influences the size and structure of the nanoparticles. Boehmite occurs as agglomerates of lamellar particles with a size of 5–10 μm.

The particle shapes and sizes of the copper compounds are different for both treatment methods and change after long-term aging:

Vacuum way: The size of the rounded agglomerates of CuO decreased from 80 to 500 nm to 20–50 nm, because of deagglomeration (Fig. 6, a).

Air way: The needle splices of copper carbonate hydroxide are 5–6 μm in length. They transformed into separate needle particles of 50–130 nm. A flower-like structure of the layered double hydroxides forms (Fig. 6, b).

The reasons of the particle size change are covered in subsection 3.2.

3.5. Reflectance spectra of the nanodispersed powders

The reflectance spectra of the samples after long-term aging are shown in Fig. 7.

There is a difference in the reflectance spectra for the samples, depending on preparation way that influences the phase composition. Air drying yielded the sample with a higher reflection coefficient, regardless of the spectrum range. The following patterns are observed from the reflectance spectra, namely that (i) the samples absorb the incident light in the IR range of the spectrum; and (ii) the reflection coefficient gradually increased. In the spectral range from 800 to 950 nm, the reflection coefficient is 10–14 % (vacuum drying) and 20–26 % (air drying), respectively. In the spectral range from 400 to 600 nm (visible spectral range), the reflection coefficient value of the sample after vacuum drying varies slightly and it is not more than 1 %, whereas the value of the reflection coefficient of air-dried sample is much higher (18–25 %).

The difference between the reflectance spectra of nanostructures after air and vacuum drying is as follows.

Vacuum drying: The spectral reflectance of the CuO at a wavelength of 912 nm, is 14 % [37].

Air drying: The reflectance of $Cu_2(OH)_2CO_3$ depends on the preparation method and composition and it is located in the wavelength range of 400–600 nm [38,39].

4. Conclusions

The work shows the results of long-term aging of the nanostructured binary materials produced by the method of electrochemical oxidation of copper and aluminum with alternating current (AC). The joint electrochemical oxidation of copper and aluminum leads to the formation of agglomerates of the nanoscale copper (I) oxide – aluminum hydroxide system. The primary aging (within a few days) of the electrolysis products in the electrolyte solution, leads to the formation of copper carbonates through carbon-containing atmospheric compounds to yield copper–aluminum layered double hydroxide containing carbonate ions between the layers (Cu-Al-CO_3-LDH) and copper carbonate hydroxide $Cu_2(OH)_2CO_3$.

Vacuum drying of the electrolysis product before aging prevents Cu_2O–AlOOH from carbonization to Cu-Al-CO_3-LDH. For the short-term aging processes, the coherent scattering region sizes of all copper-containing compounds were 15–20 nm. It increases to 40–50 nm after long-term aging because of sorption of water and carbonate ions. It has been found that AC electrolysis provides decomposition of carbon compounds at a lower temperature (135 °C) than conventional Cu-Al-CO_3–LDH production methods. The temperature of the Cu-Al-CO_3-LDH decomposition decreased even more (121 °C) after long-term aging owing to destabilization of the structure with increased content of carbonate ions between layers. The products of the joint electrochemical oxidation of copper and aluminum using alternating current change some of their structural properties as a result of the long-term aging processes. The results of this investigation can be applied for the development of high performance photoanodes or photocathodes in photoelectrochemical cells, e.g. for photocatalytic water splitting and enhancing the hydrogen evolution reaction. Furthermore, these materials can find application in metal oxide nanofluids where aging processes by a two-stage method can be employed in the use of various base fluids for a number of different applications. Further work aiming to achieve this is currently underway.

CRediT authorship contribution statement

Natalia V. Usoltseva: Writing – original draft, Supervision, Methodology, Investigation, Data curation. **Johannes H. Potgieter:** Writing – review & editing, Writing – original draft, Validation, Supervision, Methodology. **Vladimir V. An:** Writing – original draft, Funding

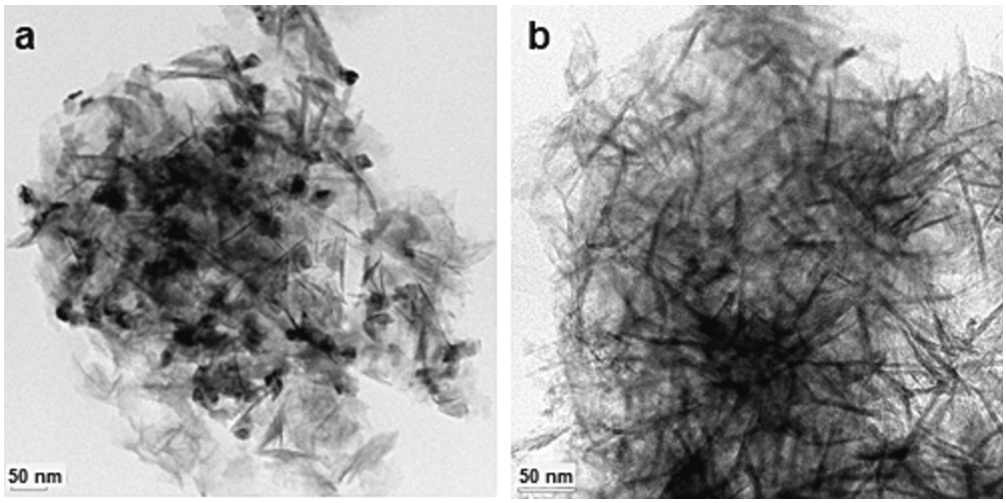

Fig. 6. TEM images of the nanodispersed materials produced by electrochemical oxidation of copper and aluminum: (a) vacuum drying, (b) air drying.

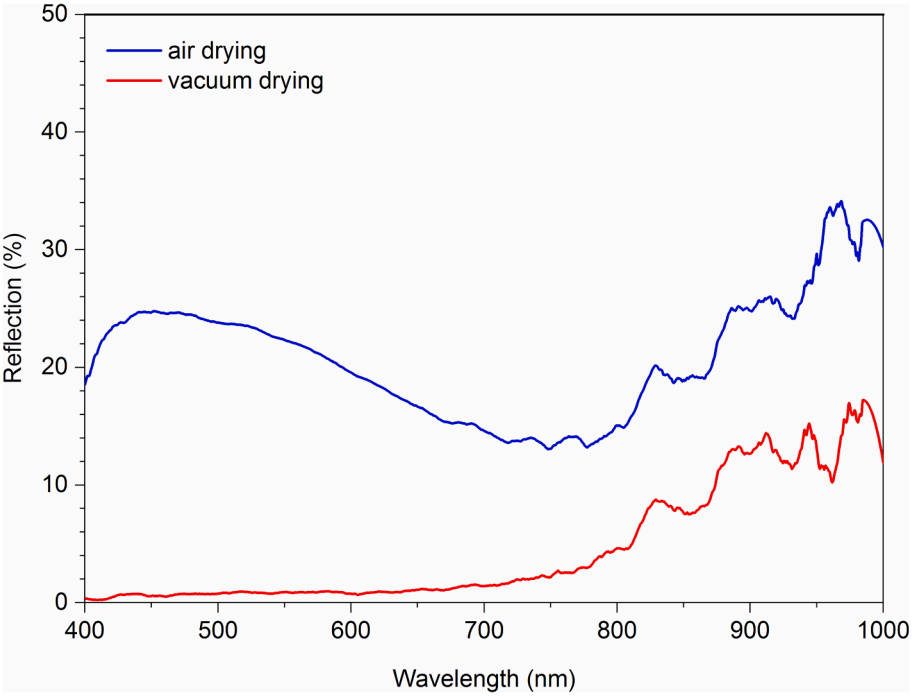

Fig. 7. Reflectance spectra of the nanodispersed materials produced by electrochemical oxidation of copper and aluminum.

acquisition, Conceptualization. **Baodan Liu:** Writing – original draft, Validation, Supervision, Methodology. **Sergey A. Stepanov:** Validation, Methodology, Investigation, Formal analysis, Data curation. **Damir T. Valiev:** Writing – original draft, Visualization, Methodology, Formal analysis.

Declaration of competing interest

The authors declare that they have no known competing financial interests or personal relationships that could have appeared to influence the work reported in this paper.

Data availability

Data will be made available on request.

Acknowledgements

This research was supported by TPU development program Priority 2030. The research was carried out using the equipment of the Center for Sharing Use «Nanomaterials and Nanotechnologies» of Tomsk Polytechnic University supported by the RF Ministry of Education and Science project #075-15-2021-710.

References

[1] C. Forano, T. Hibino, F. Leroux, C. Taviot-Guého, Chapter 13.1 Layered Double Hydroxides in Developments in clay science, Layered double hydroxides 1 (2006) 1021–1095, doi: 10.1016/S1572-4352(05)01039-1.
[2] F. Li, Q. Tan, D.G. Evans, X. Duan, Synthesis of carbon nanotubes using a novel catalyst derived from hydrotalcite-like Co–Al layered double hydroxide precursor, Catal. Lett. 99 (2005) 151–156, https://doi.org/10.1007/s10562-005-2107-7.
[3] A. Alejandre, F. Medina, X. Rodriguez, P. Salagre, Y. Cesteros, J.E. Sueiras, Cu/Ni/Al layered double hydroxides as precursors of catalysts for the wet air oxidation of phenol aqueous solutions, Appl. Catal. B: Environmental 30 (2001) 195–207, https://doi.org/10.1016/S0926-3373(00)00233-2.
[4] P.C. Pavan, G.A. Gomes, J.B. Valim, Adsorption of sodium dodecyl sulfate on layered double hydroxides, Micropor. Mesopor. Mater. 21 (1998) 659–665, https://doi.org/10.1016/S1387-1811(98)00054-7.
[5] R. Chitrakar, S. Tezuka, A. Sonoda, K. Sakane, K. Ooi, T. Hirotsu, Adsorption of phosphate from seawater on calcined Mg/Mn-layered double hydroxides, J. Colloid. Interface. Sci. 290 (2005) 45–51, https://doi.org/10.1016/j.jcis.2005.04.025.
[6] H. Tagaya, A. Ogata, T. Kuwahara, S. Ogata, M. Karasu, J. Kadokawa, K. Chiba, Intercalation of colored organic anions into insulator host lattices of layered double hydroxides, Micropor Mater. 7 (1996) 151–158, https://doi.org/10.1016/0927-6513(96)00013-2.
[7] J.-H. Choy, S.-J. Choi, J.-M. Oh, T. Park, Clay minerals and layered double hydroxides for novel biological applications, Appl. Clay Sci. 36 (2007) 122–132, https://doi.org/10.1016/j.clay.2006.07.007.
[8] J.-H. Choy, S.-Y. Kwak, J.-S. Park, Y.-J. Jeong, J. Portier, Intercalative nanohybrids of nucleoside monophosphates and DNA in layered metal hydroxide, J. Am. Chem. Soc. 121 (1999) 1399–1400, https://doi.org/10.1021/ja981823f.
[9] R.S. Jayashree, P.V. Kamath, Layered double hydroxides of ni with cr and mn as candidate electrode materials for alkaline secondary cells, J. Power Sources 107 (2002) 120–124, https://doi.org/10.1016/S0378-7753(01)00994-6.
[10] X.M. Liu, Y.H. Zhang, X.G. Zhang, S.Y. Fu, Studies on Me/Al-layered double hydroxides (me, ni and co) as electrode materials for electrochemical capacitors, Electrochim. Acta 49 (2004) 3137–3141, https://doi.org/10.1016/j.electacta.2004.02.028.
[11] C. Nyambo, C.A. Wilkie, Layered double hydroxides intercalated with borate anions: fire and thermal properties in ethylene vinyl acetate copolymer, Polym. Degrad. Stabil. 94 (2009) 506–512.
[12] C. Manzi-Nshuti, D. Wang, J.M. Hossenlopp, C.A. Wilkie, Aluminum-containing layered double hydroxides: the thermal, mechanical, and fire properties of (nano) composites of poly(methyl methacrylate), J. Mater. Chem. 18 (2008) 3091–3102, https://doi.org/10.1039/B802553C.
[13] K. Iwase, T. Hirano, I. Honma, Copper aluminum layered double hydroxides with different compositions and morphologies as electrocatalysts for the carbon dioxide reduction reaction, ChemSusChem 15 (2022) e202102340.
[14] M.H. Tajuddin, N. Yusof, I.W. Azelee, W.N.W. Salleh, A.F. Ismail, J. Jaafar, F. Aziz, K. Nagai, N.F. Razali, Development of copper-aluminum layered double hydroxide in thin film nanocomposite nanofiltration membrane for water purification process, Front. Chem. 7 (2019) 3, https://doi.org/10.3389/fchem.2019.00003.
[15] M.V. Bukhtiyarova, O.A. Bulavchenko, A.V. Bukhtiyarov, A.L. Nuzhdin, G.A. Bukhtiyarova, (2022). Selective Hydrogenation of 5-Acetoxymethylfurfural over Cu-Based Catalysts in a Flow Reactor: Effect of Cu-Al Layered Double Hydroxides Synthesis Conditions on Catalytic Properties, Catalysts 12(8) (2022) 878, 10.3390/catal12080878.
[16] X. Peng, M. Wang, F. Hu, F. Qiu, T. Zhang, H. Dai, Z. Cao, Multipath fabrication of hierarchical CuAl layered double hydroxide/carbon fiber composites for the degradation of ammonia nitrogen, J. Environ. Manage. 220 (2018) 173–182, https://doi.org/10.1016/j.jenvman.2018.05.037.
[17] A.K. Mishra, A. Roldan, N.H. de Leeuw, CuO surfaces and CO2 activation: a dispersion-corrected DFT+U study, J. Phys. Chem. C 120 (2016) 2198–2214, https://doi.org/10.1021/acs.jpcc.5b10431.
[18] C.h. Su, D.L. Suarez, In situ infrared speciation of adsorbed carbonate on aluminum and iron oxides, Clay Clay Miner. 45 (1997) 814–825.
[19] Y. Zhao, F. Xiao, Q. Jiao, Hydrothermal synthesis of Ni/Al layered double hydroxide nanorods, J. Nanotechnol. 646409 (2011), https://doi.org/10.1155/2011/646409.

[20] Y. Zhao, F. Li, R. Zhang, D.G. Evans, X. Duan, Preparation of layered double-hydroxide nanomaterials with a uniform crystallite size using a new method involving separate nucleation and aging steps, Chem. Mater. 14 (2002) 4286–4291, https://doi.org/10.1021/cm020370h.
[21] M.A. Iqbal, M. Fedel, Effect of synthesis conditions on the controlled growth of MGAL–LDH corrosion resistance film: structure and corrosion resistance properties, Coatings 9 (2019) 30, https://doi.org/10.3390/coatings9010030.
[22] V.V. Korobochkin, M.A. Balmashnov, D.A. Gorlushko, N.V. Usoltseva, V. V. Bochkareva, Phase composition and pore structure of nanoparticulate tin oxides prepared by AC electrochemical synthesis, Inorg. Mater. 49 (2013) 993–999.
[23] V. An, H. Potgieter, N. Usoltseva, D. Valiev, S. Stepanov, A. Pustovalov, A. Baryshnikov, M. Titov, A. Dolinina, MoS_2@ZnO nanoheterostructures prepared by electrospark erosion for photocatalytic applications, Nanomaterials 11 (2021) 157, https://doi.org/10.3390/nano11010157.
[24] V.V. Korobochkin, J.H. Potgieter, N.V. Usoltseva, A.S. Dolinina, V.V. An, Thermal preparation and characterization of nanodispersed copper-containing powders produced by non-equilibrium electrochemical oxidation of metals, Solid State Sci. 108 (2020) 106434, https://doi.org/10.1016/j.solidstatesciences.2020.106434.
[25] McCafferty E. Introduction to Corrosion Science. Springer Science+Business Media, 2010, New York, 575 p., 10.1007/978-1-4419-0455-3.
[26] Budavari, S. (ed.). The Merck Index - An Encyclopedia of Chemicals, Drugs, and Biologicals. Whitehouse Station, NJ: Merck and Co., Inc., 1996.
[27] K. Barbalace, Periodic table of elements - sorted by ionic radius, Environ. Chem. Com. (1995–2023,). https://EnvironmentalChemistry.com/yogi/periodic/ionicradius.html.
[28] Y. Lwin, M.A. Yarmo, Z. Yaako, Synthesis and characterization of Cu–Al layered double hydroxides, Mater. Res. Bull. 36 (2001) 193–198, https://doi.org/10.1016/S0025-5408(01)00491-3.
[29] W. Jang, S. Yoon, J. Song, J. Kim, Selective phase transformation of layered double hydroxides into mixed metal oxides for catalytic CO oxidation, Cell Reports Physical Science 2 (2021) 100628, https://doi.org/10.1016/j.xcrp.2021.100628.
[30] M. Schmidt, H.D. Lutz, Hydrogen bonding in basic copper salts: a spectroscopic study of malachite, Cu2(OH)2CO3, and brochantite, Cu4(OH)6SO4, Phys. Chem. Minerals 20 (1) (1993) 27–32.
[31] G.D. Chukin, Structure of the surface of γ-alumina, J. Struct. Chem. 17 (1976) 99–104.
[32] N.V. Usoltseva, V.V. Korobochkin, M.A. Balmashnov, Air carbonisation of AC electrochemical copper and aluminium oxidation products, Int. J. Eng. Res. Tech. 2 (2013) 2355–2362.
[33] B. Ingham, X-ray scattering characterisation of nanoparticles. Crystall. Rev. 21 (2015) 229–303, 10.17586/2220-8054-2018-9-3-364-369.
[34] N.T.T. Ha, V.T.M. Hue, B.C. Trinh, N.N. Ha, L.M. Cam, Study on the adsorption and activation behaviours of carbon dioxide over copper cluster (cu-4) and alumina-supported copper catalyst (cu-4/Al2O3) by means of density functional theory, J. Chem. 4341056 (2019), https://doi.org/10.1155/2019/4341056.
[35] Wan Nor Roslam Wan Isahak, Zatil Amali Che Ramli, Mohamad Wafiuddin Ismail, Khomah Ismail, Rahimi M. Yusop, Mohamed Wahab Mohamed Hisham, Mohd Ambar Yarmo, Adsorption–desorption of CO_2 on different type of copper oxides surfaces: Physical and chemical attractions studies, J. CO_2 Util. 2 (2013) 8-15, https://doi.org/10.1016/j.jcou.2013.06.002.
[36] N.V. Usoltseva, V.V. Korobochkin, A.S. Dolinina, Pore structure of products after AC electrochemical simultaneous oxidation of copper and aluminium, Perspektivnye Materialy 3 (2016) 59–69, in Russian.
[37] G.G. Welegergs, H.G. Gebretinsae, M.G. Tsegay, C. Mtshali, N. Mongwaketsia, K. Cloete, Z.Y. Nuru, S. Dube, M. Maaza, Single-layered biosynthesized copper oxide (CuO) nanocoatings as solar-selective absorber, Appl. Sci. 13 (2023) 1867, https://doi.org/10.3390/app13031867.
[38] M. Kartsonaki, M. Koui, P. Callet, E. Cheilakou. Non destructive identification of the colouring substances on the monuments studied by colorimetry. 4th International conference on NDT. 11-14 October 2007. Chania, Crete-Creece.
[39] J. Brocchieri, L. de Viguerie, C. Sabbarese, M. Boyer, Combination of noninvasive imaging techniques to characterize pigments in buddhist thangka paintings, X-Ray Spectrom. (2020), https://doi.org/10.1002/xrs.3189.